GROUND-BASED NEAR-INFRARED IMAGING OF THE HD 141569 CIRCUMSTELLAR DISK

A. BOCCALETTI

LESIA, Observatoire de Paris-Meudon, 5 Pl. J. Janssen, 92195 Meudon, France; anthony.boccaletti@obspm.fr;
and California Institute of Technology, Pasadena, CA 91125

J.-C. AUGEREAU

CEA/Saclay, Service d'Astrophysique, France

F. MARCHIS

University of California, Berkeley, CA 94720

AND

J. HAHN

Lunar and Planetary Institute, Houston, TX 77058

ABSTRACT

We present the first ground-based near-infrared image of the circumstellar disk around the post–Herbig Ae/Be star HD 141569A initially detected with the *Hubble Space Telescope* (*HST*). Observations were carried out in the near-IR (2.2 μm) at the Palomar 200 inch telescope using the adaptive optics system PALAO. The main large-scale asymmetric features of the disk are detected on our ground-based data. In addition, we measured that the surface brightness of the disk is slightly different than that derived by *HST* observations (at 1.1 and 1.6 μm). We interpret this possible color effect in terms of dust properties and derive a minimal grain size of 0.6 ± 0.2 μm for compact grains and a power-law index for the grain size distribution smaller than -3. Basic dynamical considerations are consistent with the presence of a remnant amount of gas in the disk.

Subject headings: circumstellar matter — instrumentation: high angular resolution —
stars: individual (HD 141569A) — techniques: image processing

1. INTRODUCTION

A circumstellar disk around the star HD 141569A was detected independently by Augereau et al. (1999a) and Weinberger et al. (1999) using the near-IR camera NIC-MOS2 on the *Hubble Space Telescope* (*HST*). These first images revealed an optically thin annular disk with a complex morphology: (1) an annular structure peaking at 325 AU, evidenced at 1.1 μm and 1.6 μm; (2) a second axisymmetric ring at 185 AU, unambiguously detected at 1.1 μm and less obvious in the 1.6 μm image. More recent data obtained with STIS in the visible wavelengths confirm the presence of two grain populations but also exhibit some strong asymmetries, especially in the closer annular pattern (arc-like patterns, for instance), with an unprecedented angular resolution (Mouillet et al. 2001). According to Mouillet et al. (2001), the anisotropic scattering of the light cannot account alone for asymmetric features and one has to invoke a nonaxisymmetric distribution of dust very likely provided by the gravitational influence of perturber(s) within the disk (a hypothetical planetary companion, for instance), outside the disk (the two stellar companions lying at 1065 and 1370 AU from the star if they are in the disk plane), or both. Some numerical simulations are ongoing to take into account the influence of the two T Tauri–like companions (J. C. Augereau et al. 2003, in preparation).

In addition, a close mid-IR emission previously inferred by spectral energy distribution fitting (Augereau et al. 1999a) was detected within 100 AU (Fisher et al. 2000) with the Keck telescope at 10.8 μm and 18.2 μm. The complex environment of HD 141569A clearly indicates that this star is in an advanced stage of evolution and may have already experienced a planetary formation stage.

We used the star HD 141569A as a fiducial case to assess the capability of the adaptive optics system at the Palomar 200 inch telescope to detect circumstellar disks around relatively young stars. Consequently, we report the first ground-based imaging of this disk in scattered light at near-IR wavelengths. Despite a much lower sensitivity than the *HST*, our data feature a better angular resolution of 0″11 (instead of 0″19 for the *HST*) at 2.2 μm in the *K* band.

The observing sequence and the data reduction process are detailed in § 2 and the subsequent results are analyzed in § 3. We discuss the possible impact on the grain properties in § 4.

2. OBSERVATION AND DATA REDUCTION

The observations of HD 1414569A (B9 V, $V = 7.0$, $K = 6.82$, $d = 99$ pc) were carried out at the Palomar 200 inch telescope using PALAO, the 241-actuators Adaptive Optics (AO) system installed at the Cassegrain focus (Troy et al. 2001), and PHARO, the near-IR camera (Hayward et al. 2001). The system can reach an average Strehl ratio of about 50% for bright stars ($m_v < 7$) under 1″ seeing at near-IR wavelengths, and Strehl ratio as high as 68% have been occasionally obtained with very good seeing.

HD 141569A was observed on 2001 May 9 and 10 with a Ks filter (2.2 μm) and a 25 mas pixel^{-1} plate scale. A coronagraphic Lyot mask (0″91 in diameter) was used to attenuate the diffraction pattern of the central star. In addition to the mask, an adequate cold Lyot stop undersizing the pupil was implemented inside the cryostat of the camera. This stop is mandatory to remove the unwanted starlight at the edges of the geometric pupil and to effectively improve the detection

of faint circumstellar material. The coronagraphic PSF was calibrated in four sequences going back and forth between both the target star and an angularly close reference star of similar spectral type and magnitude (HD 142864, A0 V, $V = 7.2$, $K = 7.2$). The visible magnitude as well as the near-IR magnitude of this PSF calibrator are optimized to benefit from the same AO correction but also to obtain a similar signal to noise ratio in the IR images. Individual images of both the star and the reference were separately recentered and finally co-added to provide an actual integration time of 1090 s, although the telescope time required to perform this thorough calibration amounts to about 2.5 hr. The target star was observed 10 minutes per sequence (including readout of the detector and sky calibration), but it took about 5 to 10 minutes to repoint the telescope in order to accurately recenter the calibrator onto the mask. The average Strehl ratio was only of 16% during the observation of HD 141569 and was measured on the HD 141569 companions (7″.5 away). The data obtained on 2001 May 10 were not usable, since the mask centering and the AO performance were poor.

At this point, the circumstellar disk is not yet detectable and a specific reduction process is necessary for the extraction of faint circumstellar material. In order to compare our data with previous *HST* observations, we used the data reduction technique described in Augereau et al. (1999a). First of all, the data for both the star and the PSF calibrator were reduced with standard procedure: bad pixel correction, flat field correction, and sky subtraction. Then, before being subtracted, the PSF calibrator needs to be recentered and scaled to the intensity of the star. We estimate the scaling factor on the ratio of the target star image to that of the calibrator. As indicated in Augereau et al. (1999a), the region ranging from 1″ to 2″ is relatively free of detected circumstellar dust and the ratio is almost constant for any orientation angle (Fig. 1). The global scaling factor is therefore estimated in this area, and we adopt a value of 0.94 ± 0.02. The uncertainty in the scaling factor is derived from the pixel-to-pixel dispersion in the same annulus (see Fig. 1). The resulting subtracted images are shown in Figure 2.

3. DATA ANALYSIS

After subtracting the calibrator, as explained above, it is still difficult to disentangle between circumstellar material and the diffraction residuals. Because the subtraction process is not perfect, the stellar diffracted light dominates at close angular distance ($r < 1″.5$). However, it was possible to unambiguously identify the circumstellar component by comparing our image with the ones obtained using the *HST* (especially with STIS). We then numerically canceled the diffraction residuals on our image and we assumed that no information can be retrieved in that particular central region.

The global elliptical shape of the disk and the presence of two asymmetric rings are now becoming obvious in Figure 2, and several major features in agreement with *HST* images can be identified. For comparison, Figure 3 shows the STIS image (Mouillet et al. 2001) with the same pixel scale and orientation angle. The regions labeled on Figure 2*b* are in very good concordance with Figure 3 (especially the NE and SW part of the inner ring), although the angular resolution and the sensitivity are lower on Palomar data. The ratio between the major and the minor axis is 1.60 ± 0.15
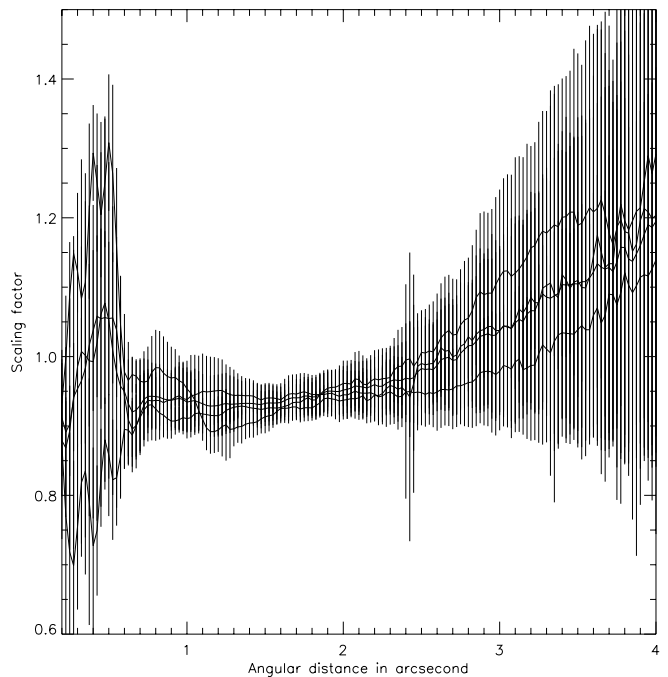

Fig. 1.—Azimuthally averaged profile of the ratio of the target star image to that of the calibrator obtained in four different regions (P.A. = 130°, 234°, 174°, and 135°). The error bars represent the azimuthal intensity dispersion inside each regions. The scaling factor is estimated between 1″ and 2″ from the central star for which the ratio is almost constant and yields a value of 0.94 ± 0.02.

corresponding to an inclination of $5°.13^{+3°.8}_{-4°.9}$ from pole-on assuming a circular disk (in agreement with previous measurements). Pieces of two independent rings are actually discernible in the disk. The external ring is peaking at 325 AU and was initially detected by Augereau et al. (1999a) and Weinberger et al. (1999). The inner ring is located at 185 AU but is slightly offset by 0″.25 ($\approx 2.5\lambda/D$) to the west as already pointed out by Mouillet et al. (2001). It is, however, difficult to have confidence in this value since only two pieces of the inner ring are visible on our data and the fitting of an ellipse is somewhat uncertain as the location of the star behind the occulting mask. More accurate measurements will be required to confirm this assumption. In addition, an extended emission detected with STIS is roughly visible to the north in Figure 2 but the presence of the two companions as well as the brightness of the background strongly limit the detection in this area. The west part of the outer ring (ranging from about P.A. = 225° to P.A. = 310°) is significantly dimmer than the eastern region by about a factor of 2. This can be partly explained by a combination of the inclination of the disk with respect to the line of sight and anisotropic scattering properties of the dust grains. But the present data, like NICMOS2 and STIS images, exhibit some broken elliptical rings with strong azimuthal asymmetries (especially in the inner ring). Mouillet et al. (2001) concluded that a nonaxisymmetric dust distribution was needed to account for the observed brightness asymmetries.

To obtain more quantitative comparisons with *HST* data the subtracted image was azimuthally averaged in several regions to derive the local surface brightness (SB) of the disk. We considered the same regions as Augereau et al. (1999a) and Mouillet et al. (2001) for accurate comparison (P.A. = 130°, 180°, 18°, 215°). First of all, the image was
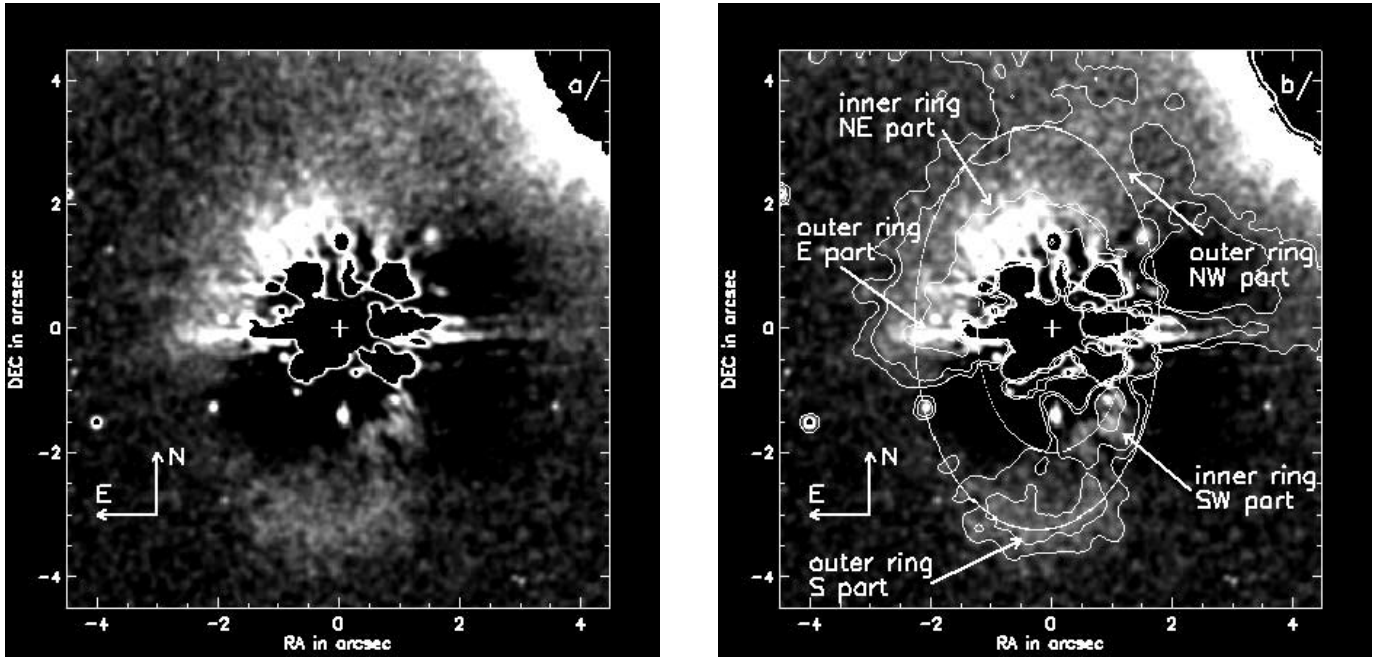
Fig. 2.—Final image of HD 141569 subtracted with a reference star (*a*). Two ellipses are over-plotted on the sub-frame (*b*) in order to emphasize the presence of the inner and outer rings. The main regions we are discussing in this paper are also indicated. The very bright area at the upper right corner is provided by the T Tauri companions. The cross at the center of the image shows the approximate location of the star HD 141569. The dark regions were numerically cancelled to remove the bright diffraction residuals.

deprojected in order to average the pixels at the same physical distance from the star. The surface brightness displayed in mJy arcsec^{-2} assumes $K = 6.99$ for the central star (as measured in our Ks filter) and a 0 mag corresponding to a flux density of 667 Jy.

To evidence the asymmetries of the inner and the outer rings the surface brightness is plotted on Figure 4 as a function of the position angle at respectively $r = 1{.}''8$ and

$r = 3{.}''2$, where r denotes the distance from the star in the deprojected image of the disk. Giving I_{max} and I_{min} the maximal and minimal intensity of the azimuthal profiles presented on Figure 4, the contrast is defined with the following relation:

$$C = \frac{I_{max} - I_{min}}{I_{max} + I_{min}} \; .$$

The contrast is as large as 98% in the inner ring ($1{.}''8$) between the bright northeast feature at P.A. $= 20°$ and the depleted southeast region at P.A. $= 130°$. The outer ring has a lower contrast of 71% between the eastern part (P.A. $= 90°$) and the southwest region around P.A. $= 230°$.

Figure 5 compares the surface brightness of the disk in the southern extension with the southeast extension. The outer ring is predominant to the inner one in these regions. The southeast part appears dimmer by a factor 1.49 ± 0.35 in the range $3''$–$3{.}''5$. This disk extension was totally or partially occulted by the wedge on STIS data and by spider diffraction spikes on NICMOS2 data. We also found a difference of surface brightness in the southern extension between our 2.2 μm data and the *HST* 1.6 μm data obtained by Augereau et al. (1999a). The peak of the southern extension on *HST* image [SB(1.6 μm)] is 1.33 ± 0.15 times brighter than in the K band [SB(2.2 μm)] as measured on our data (assuming a scaling factor of 0.94). This difference is discussed in the next section in terms of scattering properties of the dust grains.

The surface brightness of the inner ring is best evidenced in Figure 6. Although the position of the ring is in agreement with the *HST* data, it remains difficult to compare the photometry since the *HST* image was actually averaged over 360° by Weinberger et al. (1999) to derive the surface brightness at 1.1 μm. But once our data are processed in the same way we find that the ring peaks at
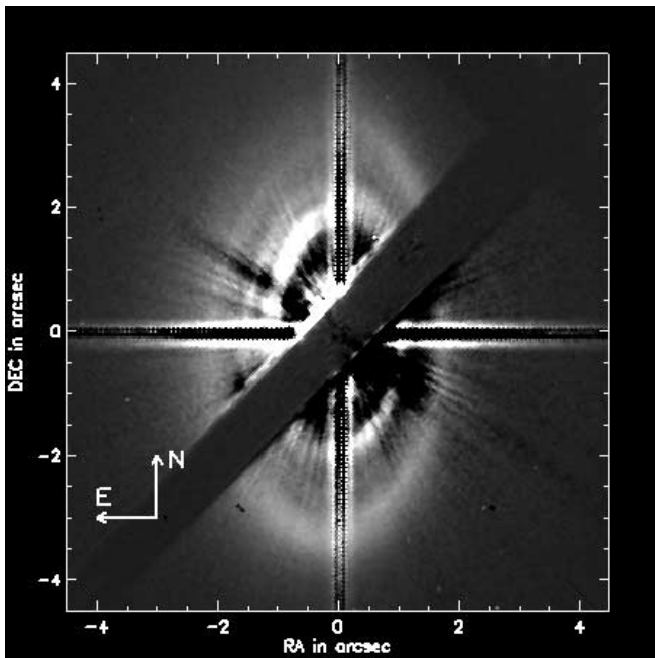

Fig. 3.—Image of HD 141569 obtained with STIS on *HST* in the visible and using the 1″ wedge mask. By courtesy of David Mouillet.
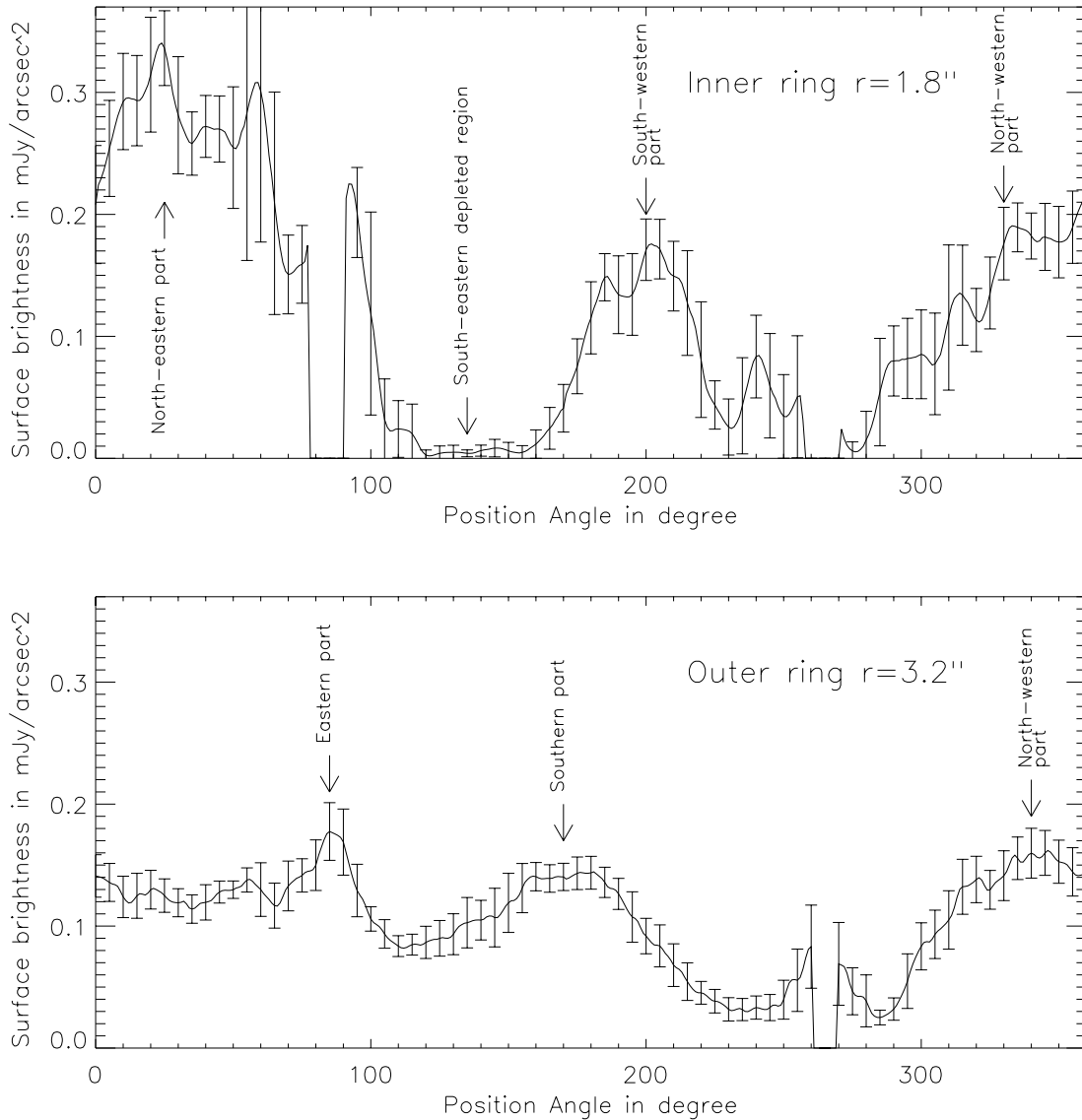
Fig. 4.—Variation of the surface brightness across the inner ring (*top*) and the outer ring (*bottom*) as a function of the position angle. The contrast of the asymmetries is as large as 98% in the inner ring and 71% in the outer ring.

0.116 ± 0.030 mJy arcsec^{-2} instead of 0.270 ± 0.020 mJy arcsec^{-2} obtained by Weinberger et al. (1999). The large amount of diffracted light at this angular separation is mostly responsible for the 25% uncertainty measured on the surface brightness at 2.2 μm.

Finally, the image displayed on Figure 2a shows some kind of clumps within and outside of the disk. Although the common hypothesis to account for the disk asymmetries is the presence of gravitational perturbers these pattern are probably not real. They likely originate in the Fourier filtering applied to smooth the high-frequency noise in the raw data.

4. IMPLICATIONS ON DISK AND GRAINS PROPERTIES

4.1. *A Possible Color Effect*

In this section we assume that the color effect revealed in Figures 5 and 6 is real and we infer a possible implication on the properties of the grains. Since the HD 141569 disk is optically thin ($L_{\rm disk}/L_* = 8.4 \times 10^{-3}$, Zuckerman et al. 1995; see also § 4.2), the wavelength dependence of the surface brightness (SB) is proportional to the star flux $\Phi^*(\lambda)$ and the scattering cross section averaged over the grain size distribution $\langle\sigma_{\rm sca}(\lambda)\rangle$ (Augereau et al. 2001). We then tried to investigate whether the observed difference of brightness between *HST* data and Palomar images is caused by the star flux only or reveals a color effect of the grains. In the following we investigate the ratio:

$$\frac{\langle\sigma_{\rm sca}(\lambda_1)\rangle}{\langle\sigma_{\rm sca}(\lambda_2)\rangle} = \frac{{\rm SB}(\lambda_1)/\Phi^*(\lambda_1)}{{\rm SB}(\lambda_2)/\Phi^*(\lambda_2)} \qquad (1)$$

with $\lambda_1 = 1.1$ or 1.6 μm and $\lambda_2 = 2.2$ μm. A deviation of this ratio from 1 reveals a nongray scattering behavior of the grains.

Assuming a B9 V spectrum for the star, we found $\Phi^*(1.6~\mu{\rm m})/\Phi^*(2.2~\mu{\rm m}) = 1.656$. The uncertainty on the ratio $\langle\sigma_{\rm sca}(1.6~\mu{\rm m})\rangle/\langle\sigma_{\rm sca}(2.2~\mu{\rm m})\rangle$ at 3″2 is related to the surface brightness uncertainty as defined above in § 3
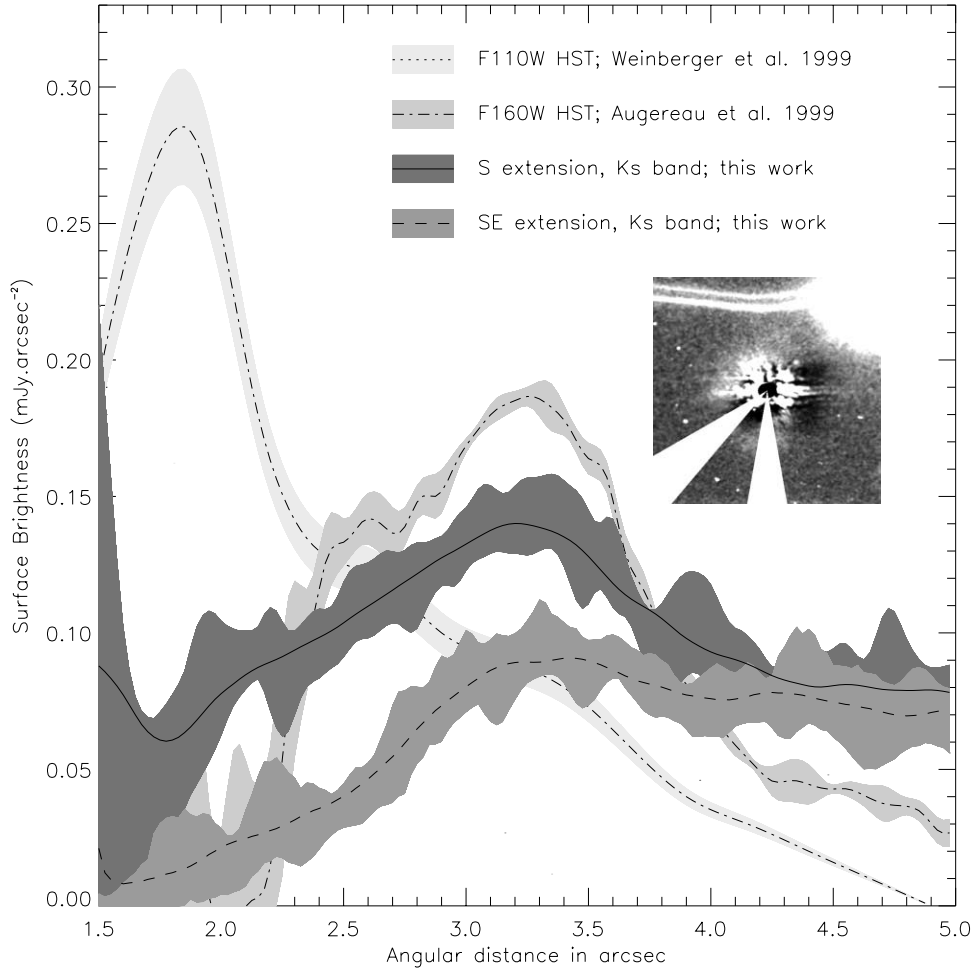
Fig. 5.—Surface brightness profile of the southern region (P.A. = $180° \pm 10°$) and the South-East region (P.A. = $130° \pm 10°$) compared to the surface brightness of the disk obtained with NICMOS at 1.1 μm (Weinberger et al. 1999) and at 1.6 μm (Augereau et al. 1999a). The captioned image shows the azimuthally averaged regions around the star on Palomar and *HST* 1.6 μm data. The brightness profile at 1.1 μm is a rough estimation of the Fig. 2 displayed in Weinberger et al. (1999) and is obtained by averaging over 360°. The profile at 1.6 μm is obtained with real data obtained by Augereau et al. (1999a).

$[\text{SB}(1.6\ \mu\text{m})/\text{SB}(2.2\ \mu\text{m}) = 1.33 \pm 0.15]$:

$$0.713 = \frac{1.33 - 0.15}{1.656} < \frac{\langle \sigma_{\text{sca}}(1.6\ \mu\text{m})\rangle}{\langle \sigma_{\text{sca}}(2.2\ \mu\text{m})\rangle} < \frac{1.33 + 0.15}{1.656} = 0.894\ . \tag{2}$$

These limits have been compared with numerical simulations in order to estimate the minimal size of the grains. We first assumed a collisional differential grain size distribution proportional to $a^{-\kappa}$ with $\kappa = 3.5$ and a minimum size $a_{\min}$ (e.g., Hellyer 1970). The use of this size distribution is justified by the short collision timescales of the observed dust grains (see next paragraph). Figure 7 shows the theoretical ratio of the averaged scattering cross sections $\langle \sigma_{\text{sca}}(1.6\ \mu\text{m})\rangle/\langle \sigma_{\text{sca}}(2.2\mu\ \text{m})\rangle$ as a function of the minimal grain size $a_{\min}$ for three porosities $P = 0$, 0.5 and 0.95 and for typical chemical compositions. Although the lower limit (0.713) of equation (2) is unhelpful in that case, the upper limit (0.894) brings some constraints on the grain size distribution. In particular we found that the minimal size of compact grains ($P = 0$) is $a_{\min} \simeq 0.6 \pm 0.2\ \mu$m. This minimal size increases with the porosity and scales approximately with $(1 - P)^{-1}$: $a_{\min} \simeq 1.5 \pm 0.5\ \mu$m for $P = 0.5$, and $a_{\min} \simeq 16 \pm 9\ \mu$m for $P = 0.95$. However, in this calculation we

used an averaged scaling factor of 0.94 and the grain size distribution is no longer constrained if we also consider the scaling factor uncertainty (0.94 ± 0.02).

The same approach considering now the 1.1 μm *HST* data instead of the 1.6 μm measurements leads to

$$0.576 < \frac{\langle \sigma_{\text{sca}}(1.1\ \mu\text{m})\rangle}{\langle \sigma_{\text{sca}}(2.2\ \mu\text{m})\rangle} < 1.135\ , \tag{3}$$

assuming $\Phi^*(1.1\ \mu\text{m}\ )/\Phi^*(2.2\ \mu\text{m}) = 2.970$. We then obtain $a_{\min} \gtrsim 0.2 \times (1 - P)^{-1}\ \mu$m, which does not improve the accuracy but is in agreement with the previous analysis performed at 1.6 μm and 2.2 μm. The results are consistent with grains significantly larger than those in the interstellar medium or in young massive circumstellar disks (Backman & Paresce 1993). Moreover, these values do not strongly depend on the assumed size distribution as long as κ is larger than 3. For small κ values, the scattering cross section is dominated by the large grains that tend to have a gray scattering behavior not consistent with the observed color effect.

4.2. Basic Dynamical Considerations

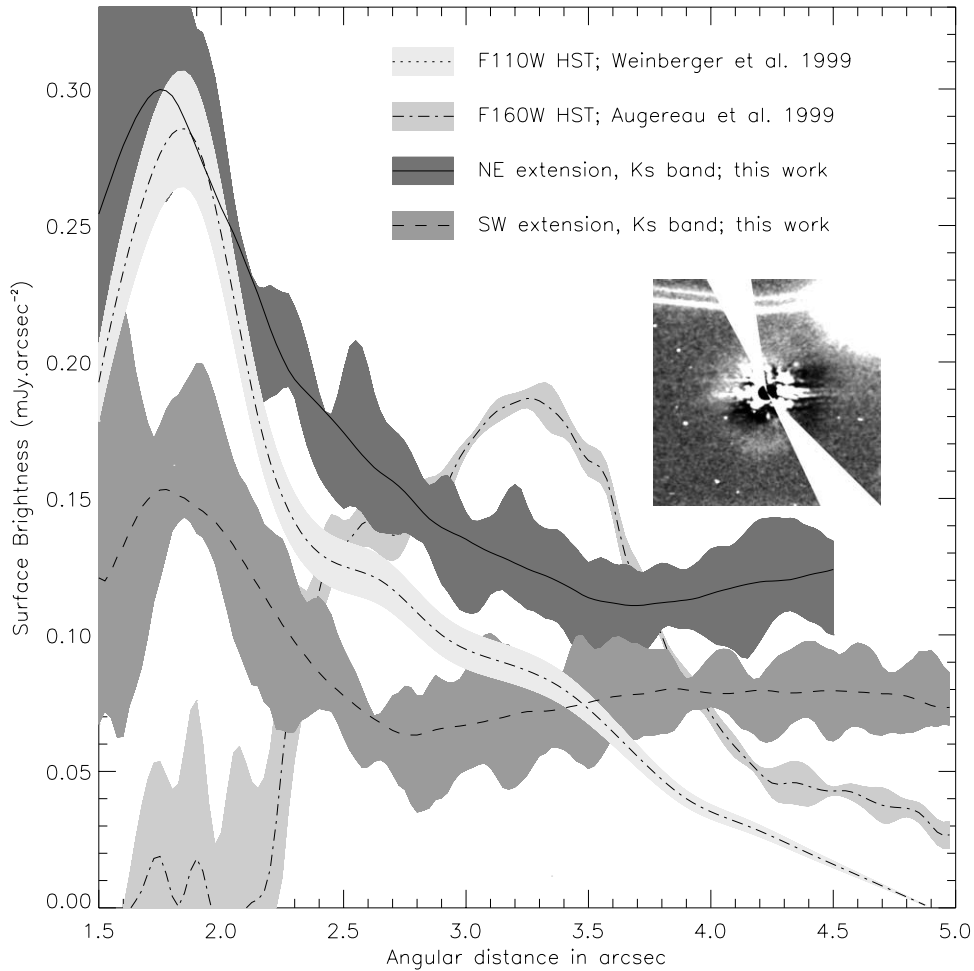Assuming circular orbits, we estimate the upper limit on the collision timescale of the observed dust grains by

Fig. 6.—Surface brightness profile of the northeast region (P.A. $= 18° \pm 10°$) and the southwest region (P.A. $= 215° \pm 10°$) compared to the surface brightness of the disk obtained with NICMOS at 1.1 μm (Weinberger et al. 1999) and at 1.6 μm (Augereau et al. 1999a). The captioned image shows the azimuthally averaged regions around the star on Palomar and *HST* 1.6 μm data. The brightness profile at 1.1 μm is a rough estimation of the Fig. 2 displayed in Weinberger et al. (1999) and is obtained by averaging over 360°. The profile at 1.6 μm is obtained with real data obtained by Augereau et al. (1999a).

the relation $t_{coll} \simeq (2\alpha\tau\Omega)^{-1}$, where $\Omega = (GM_*/r^3)^{1/2}$ is the Keplerian circular rotation frequency, $M_* = 2.3\ M_\odot$ is the star mass (van den Ancker, de Winter, & Tjin A Djie 1998), τ is the normal optical thickness of the disk in the near-IR at distance r, and α is a constant value depending on the grains optical properties, ranging typically from 0.5 to 1 in the regime of grain sizes considered here. Since the HD 141569 disk is not seen edge-on and is most certainly not geometrically thick (Mouillet et al. 2001), an estimate of τ in the near-IR can be derived from the measured surface brightness SB(r) with the simplified relation: $\tau(r) \simeq 8\pi r^2 \mathrm{SB}(r)/\Phi^*(\lambda)$ (e.g., Appendix A in Augereau et al. 2001). At 2.2 μm we derive an upper limit for the outer ring of $\tau(3\rlap{.}''2) \simeq 3.4^{+0.2}_{-1.1} \times 10^{-2}$ (southern direction) and $\tau(1\rlap{.}''8) \simeq 2.3^{+0.1}_{-0.8} \times 10^{-2}$ for the inner ring (N-NE direction). The positive uncertainty on $\tau(r)$ comes from the factor of 2 between the east and west part of the disk that can be due to anisotropic scattering properties of the grains, whereas the above relation assumes an isotropic grain scattering. This factor of 2 implies an upper limit on the asymmetry factor $|g|$ for the phase function of $\sim$0.14 in the Henyey & Greenstein (1941) approach, leading to a maximum deviation of $\sim$5% from the isotropic case for scattering angles close to 90°. The negative uncertainty of τ also relies on the optical properties of

the grains since $\tau(r)$ can be decreased by a factor of 1.5 if the minimum grain size is small compared to the wavelength (at least up to 95% of porosity). Coming back to collision timescales, we obtain $t_{coll}(3\rlap{.}''2)$ ranging from 8.7×10^3 to 1.7×10^4 yr and $t_{coll}(1\rlap{.}''8)$ from 5.4×10^3 to 1.1×10^4 yr, a few orders of magnitude less than the age of the star (8 Myr).[1]

The survival of the smallest grains in the system needs then to be considered to account for the presence of the disk. Let us first assume that the disk is free of gas. In such a case, radiation pressure efficiently blows the smallest grains out of the system on very short timescales and the outer system of HD 141569 would then be of "debris disk" type implying the presence of large bodies continuously replenishing the dust disk. Therefore, the grains observed in the near-IR and produced by collisions among large bodies are gravitationally linked to the system if their radiation pressure to gravitational forces ratio is less than 0.5 (see, e.g., Lecavelier des Etangs 1998 and references therein). This dynamical consideration, which does not depend on the distance to the star,

---

[1] Note that $(2\alpha\tau)^{-1}$ represents the typical number of orbits before a grain on a circular orbit undergoes a collision and the estimated timescales correspond to 15–30 orbits at 3$\rlap{.}''$2 and 22–44 orbits at 1$\rlap{.}''$8.
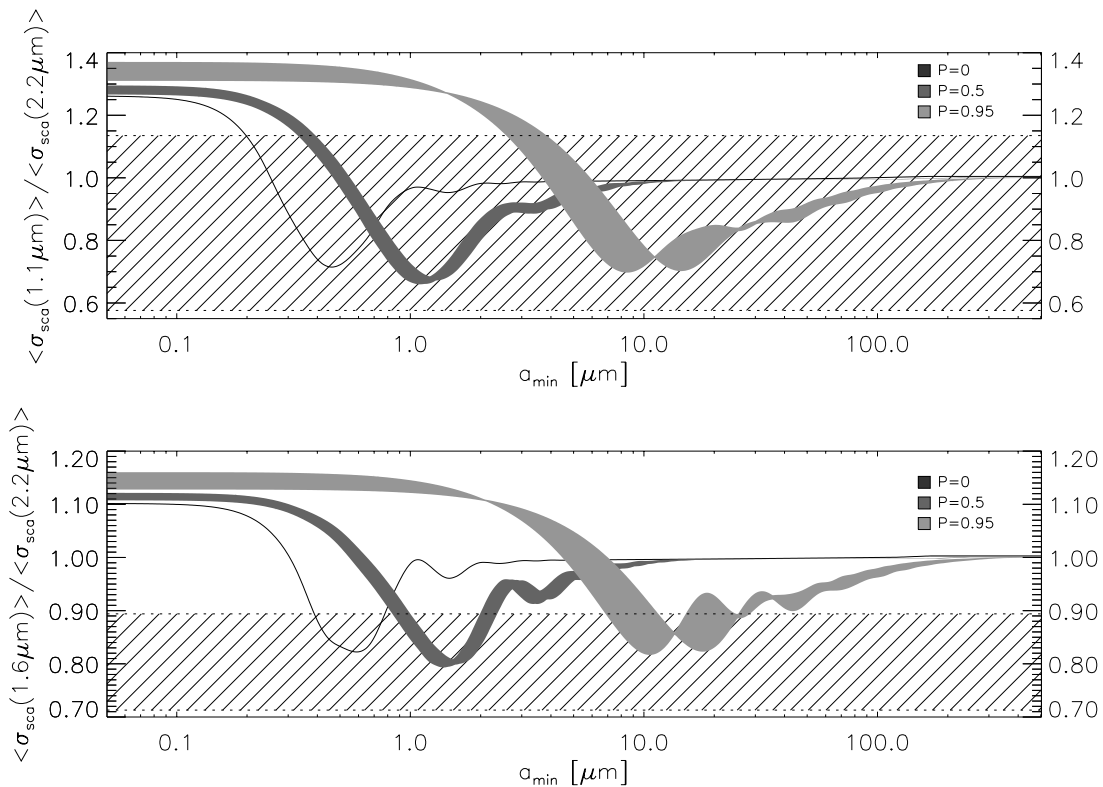
Fig. 7.—Numerical simulations of the theoretical ratios $\langle\sigma_{sca}(1.1\ \mu m)\rangle/\langle\sigma_{sca}(2.2\ \mu m)\rangle$ and $\langle\sigma_{sca}(1.6\ \mu m)\rangle/\langle\sigma_{sca}(2.2\ \mu m)\rangle$ as a function of the minimal grain size a_{min}, for three porosities $P = 0$, $P = 0.5$, and $P = 0.95$ and assuming a grain size distribution following a -3.5 power law. The following chemical compositions have been assumed: graphite, amorphous, and crystalline silicates for $P = 0, 0.5, 0.95$, mixed with organic refractories and/or water ice (10% of the vacuum due to porosity) for noncompact grains ($P = 0.5, 0.95$). The upper and lower limits derived from eq. (2) and eq. (3) are also overplotted.

directly translates into grain size constraint within the disk (e.g., Backman & Paresce 1993). A model developed by Augereau (2000) to compute the forces ratio was already applied to the analysis of HR 4796 circumstellar disk observations (Augereau et al. 1999b). It takes into account stellar parameters and grain properties. For the case of HD 141569, if the environment were free of gas, the minimum grain size in the disk would be very close to the blow-out size limit which is about $a_{min} \simeq 6\ \mu m$ if $P = 0$, $a_{min} \simeq 9\ \mu m$ if $P = 0.5$, and $a_{min} \simeq 45\ \mu m$ if $P = 0.95$ (i.e., 10 times larger than what we derived from our data). According to these results, bound grains in the HD 141569 system should therefore induce a fainter (or no) color effect (Fig. 7) than observed. If the measured color effect is realistic then grains smaller than the blow-out size limit in the absence of gas exist in the system. The assumption of the absence of gas is in fact probably not correct, since the CO $J = 2$–1 brightness temperature measured by Zuckerman et al. (1995) implies a CO abundance significantly larger than for main-sequence stars but smaller than for class II T Tauri stars. Therefore, the presence of gas is needed to allow the survival of the smallest grains. Indeed, the drag forces of the gas dominate over radiation pressure and keep the dust in orbit around the star.

5. CONCLUSION

HD 141569 was used as a fiducial target to assess the capability of the Palomar 200 inch telescope in the search for circumstellar disks. The complex structure of the dusty disk has been successfully detected at near-IR wavelengths, despite a modest Strehl ratio of only 16%. Therefore, this observation demonstrates the very good performance (comparable to that of the *HST*) of large ground-based telescopes equipped with high-order AO systems. Although a few circumstellar disks have been already imaged from the ground (β Pic or HR 4796, for instance) in the near-IR, the 200 inch telescope is to date the largest telescope equipped with a Lyot coronagraph, thus providing a large angular resolution (~90 mas in K band) together with a high dynamic range. The result of a search for substellar companion has shown that under good atmospheric seeing, the detection threshold could be as large as $\Delta m \approx 9$ mag at $0\rlap{.}''5$, $\Delta m \approx 12$ mag at $1\rlap{.}''5$, and $\Delta m \approx 14$–15 mag beyond $2''$. This capability needs to be intensively exploited to discover and further characterize other circumstellar disks.

The many independent data obtained on HD 141569 provided us with a multiwavelength analysis (visible, near-IR, and mid-IR) of this star, allowing us to derive some physical properties of the grains contained in the disk. In addition to the successful detection of the disk reported in this paper, we have shown that a careful comparison of ground-based data and *HST* data obtained, respectively, at 1.6 and 2.2 μm could bring some constraints on the grain size distribution. In particular, we derive a minimal size of $0.6 \pm 0.2\ \mu m$ for compact grains and a grain size distribution steeper than a^{-3}. Grains are then larger than those found in circumstellar disks around pre–main-sequence stars but also smaller than expected for a Vega-like system. Therefore, we conclude that the gas is probably not fully dissipated, which agrees

with the CO detection by Zuckerman et al. (1995). However, as explained in § 3, the scaling factor between the target star and the calibrator star is the major source of uncertainty in that study. Once the scaling factor uncertainty is included in the analysis, we end up with a wide range of grain size. A monitoring of the AO parameters along the observation would have been useful to characterize the level of correction on both the target star and the calibrator in order to rely on the subtraction process. Additional observations will be required to confirm the presence of a color effect and to search for gravitational perturbers.

We could certainly get more accurate results if the data were obtained with a single instrument. In that respect, the new generation of Lyot coronagraphs becoming available on both the Keck telescope and on the VLT will be definitely worthwhile for the study of circumstellar disks.

REFERENCES

Augereau, J. C. 2000, PhD thesis, Univ. Grenoble
Augereau, J. C., Lagrange, A. M., Mouillet, D., & Ménard, F. 2001, A&A, 365, 78
———— 1999a, A&A, 350, L51
Augereau, J. C., Lagrange, A. M., Mouillet, D., Papaloizou, J. C. B., & Grorod, P. A. 1999b, A&A, 348, 557
Backman, D. E., & Paresce, F. 1993, in Protostars and Planets III, ed. E. Levy, J. Lunine, & M. Matthews (Tucson: Univ. Ariz. Press), 1253
Fisher, R. S., Telesco, C. M., Piña, R. K., Knacke, R. F., & Wyatt, M. C. 2000, ApJ, 532, L141
Hayward, T. L., Brandl, B., Pirger, B., Blacken, C., Gull, G. E., Schoenwald, J., & Houck, J. R. 2001, PASP, 113, 105

Hellyer, B. 1970, MNRAS, 148, 383
Henyey, L. G., & Greenstein, J. L. 1941, ApJ, 93, 70
Lecavelier Des Etangs, A. 1998, A&A, 337, 501
Mouillet, D., Lagrange, A. M, Augereau, J. C., & Ménard, F. 2001, A&A, 372, L61
Troy, M., et al. 2000, Proc. SPIE, 4007, 31
van den Ancker, M. E., de Winter, D., & Tjin A Djie, H. R. E. 1998, A&A, 330, 145
Weinberger, A. J., Becklin, E. E., Schneider, G., Smith, B. A., Lowrance, P. J., Silverstone, M. D., Zuckerman, B., & Terrile, R. J. 1999, ApJ, 525, L53
Zuckerman, B., Kim, Sungsoo S., & Liu, T. 1995, ApJ, 446, L79